

Mapping previously undetected trees reveals overlooked changes in pan-tropical tree cover

Received: 22 July 2024

Accepted: 30 May 2025

Published online: 01 July 2025



Shidong Liu^{1,2,3,10}, Jie Zhang^{2,4,10}, Li Wang¹✉, Philippe Ciais⁵, Jianjun Zhang²✉, Josep Penuelas^{6,7}, Biswajit Nath⁸, Iskid Jacquet², Xia Wu⁹, Shengping Ding³, Wang Li¹, Ni Huang¹, Wanjuan Song¹, WenJian Ni¹ & Zheng Niu¹

Detecting tree cover is crucial for sustainable land management and climate mitigation. Here we develop an automatic detection algorithm using high-resolution satellite data (<5 m) to map pan-tropical tree cover (2015–2022), enabling identification and change analysis for previously undetected tree cover (PUTC). Our findings reveal that neglecting PUTC represents $17.31 \pm 1.78\%$ of the total pan-tropical tree cover. Tree cover net decreased by 61.05 ± 2.36 Mha in both forested areas (63.93%) and non-forested areas (36.07%) between 2015 and 2022. Intense changes in tree cover are primarily observed in regions with PUTC, where the World Cover dataset with a resolution of 10 m often fails to accurately detect tree cover. We also conduct a sensitivity analysis to quantify the contributions of climate factors and anthropogenic impacts (including human activities and land use cover change) to tree cover dynamics. Our findings indicate that 43.98% of tree cover gain is linked to increased precipitation, while 56.03% of tree cover loss is associated with anthropogenic impacts. These findings highlight the need to include undetected tree cover in strategies combating degradation, climate change, and promoting sustainability. Fine-scale mapping can improve biogeochemical cycles modeling and vegetation-climate interactions, improving global change understanding.

Climate change and human activities are increasingly affecting tree dynamics, with profound implications for global carbon stocks. Pan-tropical trees play a crucial role in global biodiversity, hydrology, climate, and carbon cycling^{1–4}. Previous studies have mainly focused on forests, which are typically defined as areas with a crown closure rate

exceeding 25% and spanning more than 0.5 hectares⁵. However, trees outside of forests, such as individual urban trees and those in woodlands and arid regions, provide obvious ecological benefits for climate mitigation and ecosystem services⁶. For instance, trees in croplands, grasslands, and deserts constitute an important but highly variable

¹State Key Laboratory of Remote Sensing and Digital Earth, Aerospace Information Research Institute, Chinese Academy of Sciences, Beijing, China. ²School of Land Science and Technology, China University of Geosciences, Beijing, China. ³Faculty of Science, University of Copenhagen, Copenhagen, Denmark. ⁴Department of Earth System Science, Ministry of Education Key Laboratory for Earth System Modeling, Institute for Global Change Studies, Tsinghua University, Beijing, China. ⁵Laboratoire des Sciences du Climat et de l'Environnement, LSCE-IPSL (CEA-CNRS-UVSQ), Université Paris-Saclay, Gif Sur Yvette, France. ⁶CREAF, Cerdanyola Del Valles, Catalonia, Spain. ⁷CSIC, Global Ecology Unit CREAF-CSIC-UAB, Bellaterra, Spain. ⁸Department of Geography and Environmental Studies, Faculty of Biological Sciences, University of Chittagong, Chittagong, Bangladesh. ⁹Geography Department, Humboldt-Universität zu Berlin, Berlin, Germany. ¹⁰These authors contributed equally: Shidong Liu, Jie Zhang. ✉e-mail: wangli@radi.ac.cn; zhangjianjun@cugb.edu.cn

carbon pool⁷. Unlike densely packed forest trees, isolated trees are less sensitive to resource competition, potentially resulting in distinct growth responses to environmental changes^{7–9}. Despite the increasingly critical role in carbon sequestration and the provision of ecosystem services, trees outside forests remain poorly quantified. Furthermore, tracking tree cover change represents a fundamental aspect of environmental science and policy¹⁰.

The quantitative assessment of trees both inside and outside forests has gained increasing attention^{10,11}. However, global forest monitoring systems remain inadequate in quantifying non-forest trees^{12–14}, with most non-forest land cover areas in pan-tropical regions being depicted as 0% tree cover^{15,16}. These classifications exclude a large proportion of scattered trees and their contributions to carbon stocks at large scales. The driver factors of tree cover dynamics remain incompletely understood, particularly for human activities' disturbance affecting trees outside forests^{17,18}, where anthropogenic losses are systematically underestimated^{19,20}. Climate change further threatens the stability of tropical forests^{20–23}. Existing research identified population density and precipitation as key indicators of human activities (planting or cutting)²⁴ and climate change (drought or humidity)^{25,26}. Therefore, a critical gap remains in mapping pan-tropical trees, hindering the analysis of ongoing changes and their drivers, thereby impeding the precise formulation and implementation of global forest management policies.

Recent advancements in deep learning have enabled more precise detection of high-resolution tree cover²⁷, particularly in regions such as Africa^{10,11}, Southeast Asian island nations²⁸, and India¹⁴. However, quantifying large-scale changes in tree cover remains a considerable challenge¹⁴. The selection of samples has high adaptability limitations in terms of location and image, that is, different spatial locations, remote sensing image shooting times, and image qualities all require the re-selection of samples^{11,29}. Variability in global climatic zones, ecosystem types, and human management practices, coupled with the spatiotemporal heterogeneity of remote sensing images, limits the transferability of deep learning models developed in specific contexts for global applications (see Supplementary Note 1). The instability of images and samples hinders the identification and mapping of high-resolution tree cover change on a large scale^{13,30}. Unlike conventional deep learning approaches, which heavily rely on manual sample selection and require substantial resources, there is an urgent need to develop an automated sampling machine learning model that leverages the inherent features of tree crowns across diverse environments.

Here, we address these limitations by mapping tree cover and its dynamics across pan-tropical regions with a resolution of <5 meters. We integrate modern decision tree classification techniques³¹ and machine learning techniques¹⁰ to segment tree canopy cover from the global Planet images, capturing both forests and individual trees, including plantations and afforestation. We redefine identifiable tree cover as woody plants with crown sizes greater than 5 m¹¹. Based on the tree cover map, we aggregate tree cover into 500 m × 500 m grid cells for statistical analysis, with land cover attributes assigned based on the MODIS MCD12Q1 Global Land Cover Products³². Additionally, we calculate the proportion of previously undetected tree cover (PUTC), by comparing our high-resolution tree cover data with existing tree cover recorded in the World Cover dataset (10 m resolution)³³. We evaluate how tree cover changes correlate with human activities, climate change, and land use cover change (LUCC) at fine spatial scales.

Results

High-resolution map of pan-tropical tree cover

We conducted validation of the tree cover by selecting over 1,50,000 sample points based on Google imagery in the Google Earth Engine (GEE) platform (see Supplementary Fig. 1). The validation results indicate that the overall accuracy of tree cover in the pan-tropical region reaches 97.31%. This includes accuracy rates of 99.03% in

forests, 96.29% in built-up areas, 96.74% in croplands, 96.93% in shrub/grassland grids, and 99.48% in bare land/deserts, across various grid types. Additionally, we computed a precision of 96.64%, a recall of 98.82%, and an F1 score of 0.9772 for both tree and non-tree regions. These accuracy metrics reflect the performance of the final mapping results of the entire model. We obtained similar validation results based on a 10 m land cover as the classification criterion for sample points (see Supplementary Table 1). The user's accuracy of tree cover identification under different grid types or land cover exceeds 95% (see Supplementary Table 2). By contrast, tree cover has a lower producer's accuracy of 95.17%, and the lowest producer's accuracy is mainly in Built-up area (86.12%) and grassland/shrubs (89.63%, see Supplementary Table 3). This accuracy is relative to images with a resolution of 5 m, and some tree canopies that are smaller and visible on Google imagery but not visible to the Planet imagery are not within the scope of this study.

The concentration of the tree cover is predominantly in forest grids dominated by tropical rainforests. However, the trees in other land cover types cannot be ignored (see Fig. 1). The total pan-tropical tree cover area reaches 2286.74 Mha, with 53.37% of the crown distributed in non-forest grids. The average tree cover ratios for each grid type from 2018 to 2020 were 88.73% in forest grids, 42.13% in shrub/grassland grids, 40.58% in built-up area grids, 29.37% in cropland grids, and 2.00% in bare land/desert grids (see Fig. 1a, b). The average tree covers in different tropical continents follow this pattern: America (63.08%) > Asia (59.13%) > Africa (34.61%). For forest grids, the average tree cover in the Americas is the largest, exceeding 90.28%, far greater than in Asia (87.65%) and Africa (85.87%) (see Fig. 1c). Cropland grids (36.35% in the Americas > 28.70% in Asia > 26.81% in Africa) and built-up area grids (45.78% in the Americas > 38.18% in Asia > 35.45% in Africa) exhibit similar characteristics. The average tree cover in grassland/shrub grids in Asia (67.92%) and that in deserts/bare land (15.26%) are much higher than that in the Americas and Africa.

Distribution of high-resolution PUTC

We obtained the proportion of PUTC by overlaying our data with the tree cover product of the World Cover dataset (see Fig. 2a, b). PUTC accounts for $17.31 \pm 1.78\%$ of all tree cover in pan-tropical (see Supplementary Fig. 2). Notably, statistics on PUTC show that the World Cover dataset in forest grids has an overestimation of 0.43% tree cover, indicating that existing forest with tree cover of 100% in World cover has a large number of ignored non-tree patches. Meanwhile, the World Cover dataset in non-forest grids has left out 17.74% of tree cover. The grid type with the highest proportion of PUTC is shrub/grassland grid (15.11%), followed by cropland (2.15%), bare land/desert (0.40%), and built-up area grid (0.08%). For forest grids, the previous dataset mislabeled non-tree cover as tree cover (Asia: 0.88%, Africa: 0.52%, America: 0.19%).

At the continental scale, Africa has the highest PUTC percentage in shrub/grassland grids, reaching 26.27%. Asia shows the highest PUTC percentage in agricultural grids, specifically 4.41%. Among non-forest grids, 5.63% in Asia, 30.03% in Africa, and 13.78% in the Americas are not accurately represented as tree cover in the previous map. Notably, Africa exhibits a higher PUTC percentage in bare land/desert grids at 0.69%. Asia's PUTC percentage in built-up area grids, at 0.69%, exceeds the pan-tropical average (see Supplementary Fig. 2). The PUTC we detected is consistent with the current high-resolution trees outside forests recognized in Africa (see Supplementary Fig. 4).

The spatiotemporal change of tree cover

From 2015 to 2022, the average tree cover density in the pan-tropical area decreased by 0.01%, with that in cropland grid, forest grid, shrub/grassland grid, bare land/desert grid, and built-up area grid changing by -0.163% , -0.113% , -0.108% , 0.0352% , and -0.147% , respectively (see Fig. 3a, b). The accuracy analysis report shows that the mapping accuracy of our tree cover change is as high as 92.47% (see

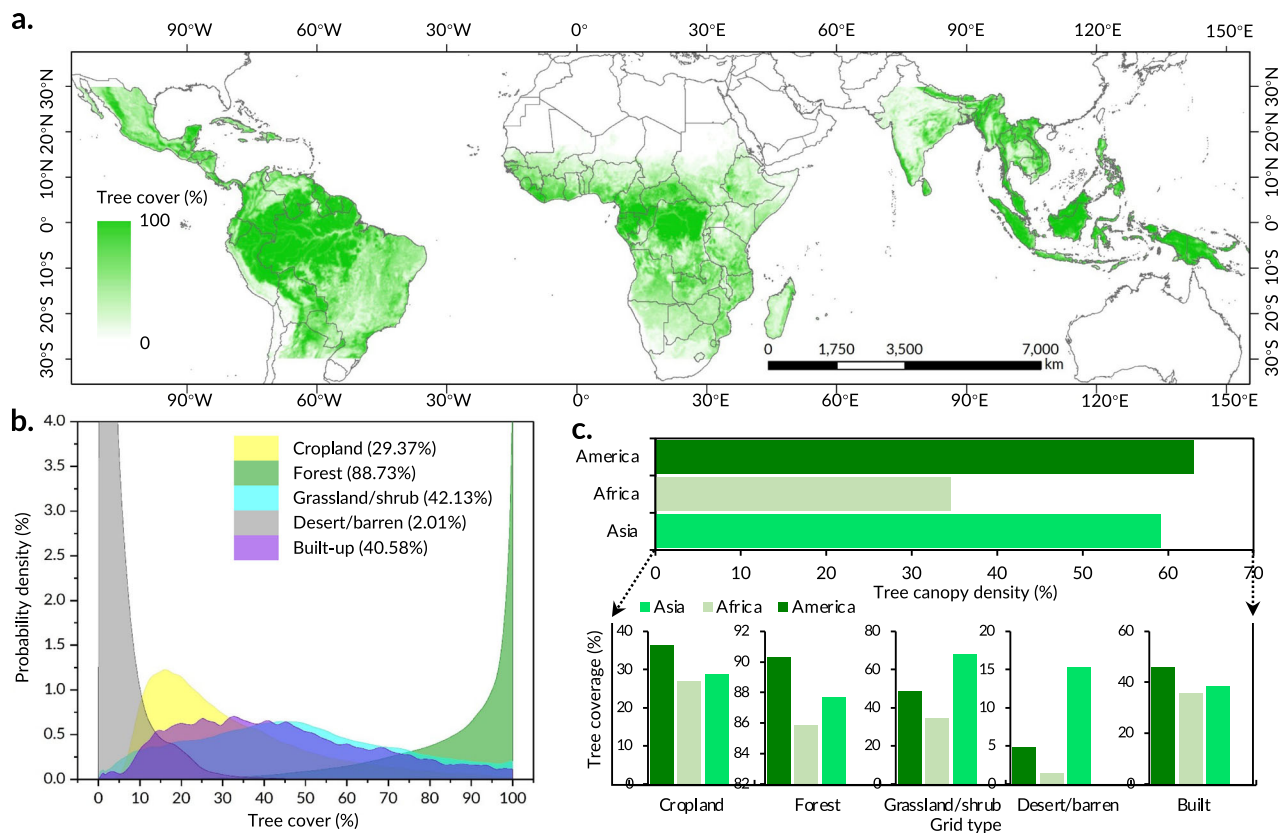


Fig. 1 | pan-tropical tree cover. **a** and **b** represent the spatial distribution of pan-tropical tree cover and that in different grid types, respectively. **c** is the proportion of pan-tropical tree cover in different grid types in different regions. Data for this figure are available at Zenodo (<https://doi.org/10.5281/zenodo.14892757>).

Supplementary Note 2). The pan-tropical tree cover gross lost by $2.94 \pm 0.09\%$ (67.24 ± 2.05 Mha). However, during the same period, the pan-tropical tree cover only gross gained by $0.27 \pm 0.11\%$ (6.19 ± 2.56 Mha), which is less than one-tenth of the loss. The area of tree cover in the pan-tropical net decreased by $2.67\% \pm 0.10\%$ (61.05 ± 2.36 Mha), with forest and non-forest grids contributing 63.93% and 36.07%, respectively (see Fig. 3c, d). Compared to the Global Forest Resources Assessment 2020 (FRA 2020) with a net loss of 4.32% (the pan-tropical total forest cover area reaches 1799Mha and decreases by an average of 7.61 Mha per year³⁴) of forest in 2010–2020 (see Supplementary Table 4 and 5), the proportion of tree cover net loss of 39.03 Mha is 3.66% in the forest grid in 2015–2022, which is consistent with the FRA2020. This small difference mainly comes from the difference in the definition of trees and the difference in periods. The area of tree cover in Asia, Africa, and the Americas also decreased by 0.83%, 2.18%, and 1.54%, respectively. Interestingly, the decrease in tree cover in non-forest grids contributed 83.81% and 58.21% to the net decrease in tree cover in Africa and the Americas, respectively. Although the area of tree cover in non-forest grids in Asia has slightly increased (0.08%), this has not changed the overall trend of declining tree cover in Asia.

The degraded areas of tree cover in space are mainly distributed around tropical rainforests and forests in Southeast Asia (see Fig. 3b). Areas with massive tree cover loss, such as Matto Grosso, Laos, and Congo, match well the Global Forest Change dataset⁵. The increased areas of tree cover in space are mainly distributed within non-forest grids or forest edge areas.

Contribution of driving factors for changes in tree cover

Notably, regions experiencing the most significant shifts in tree cover proportion, encompassing both substantial increases and decreases, are primarily located within non-forest grids exhibiting higher PUTC

ratios or forest grids characterized by a greater presence of non-tree patches (see Fig. 4 and Supplementary Fig. 7). To elucidate this relationship between PUTC ratio and tree cover changes from 2015 to 2022, we conducted a coupling analysis (see Fig. 4a). Based on their positions within the coordinate system, all changing pixels have been categorized into four groups: higher growth area (quadrant I, where PUTC higher than 0 and tree cover growth), lower growth area (quadrant II, where PUTC lower than 0 and tree cover growth) lower reduction areas (quadrant III, where PUTC lower than 0 and tree cover reduction) and higher reduction areas (quadrant IV, where PUTC higher than 0 and tree cover reduction). The proportions of changing pixels from Quadrant I to Quadrant IV are 19.26%, 1.73%, 35.04%, and 43.97%, respectively. Over 95% of grids in areas with negative PUTC ratios are concentrated in the overestimated reduction area (see Fig. 4a). Conversely, for areas with a positive PUTC ratio, 70% of grids are situated in undervalued reduction areas, with percentages reaching 76.73%, 71.85%, and 62.16% in cropland grids, built-up area grids, and shrub/grasslands grids, respectively (see Fig. 4b–f). It's noteworthy that over 91.73% of the areas exhibiting increased tree cover are located in the undervalued growth area. Additionally, the proportion of PUTC in bare/desert grids surpasses 99%, with more than 71.28% of these grids falling within undervalued growth areas.

Within forest grids, tree cover is primarily decreasing (95.46%), with 65.90% of grids located in the overestimated reduction area (see Fig. 4a). Overall, as the PUTC proportion increases, the trend in tree cover change gradually becomes positive (slope = 0.0236). This positive correlation holds across different grid types, following the pattern: shrub/grassland grids (slope = 0.0796) > cropland grids (slope = 0.0291) > forest grids (slope = 0.0031) > built-up area grids (slope = 0.0028) = bare land/desert grids (slope = 0.0028) (see Fig. 4b–f). It's noteworthy that areas experiencing significant short-term tree cover changes predominantly occur in forest grids at forest

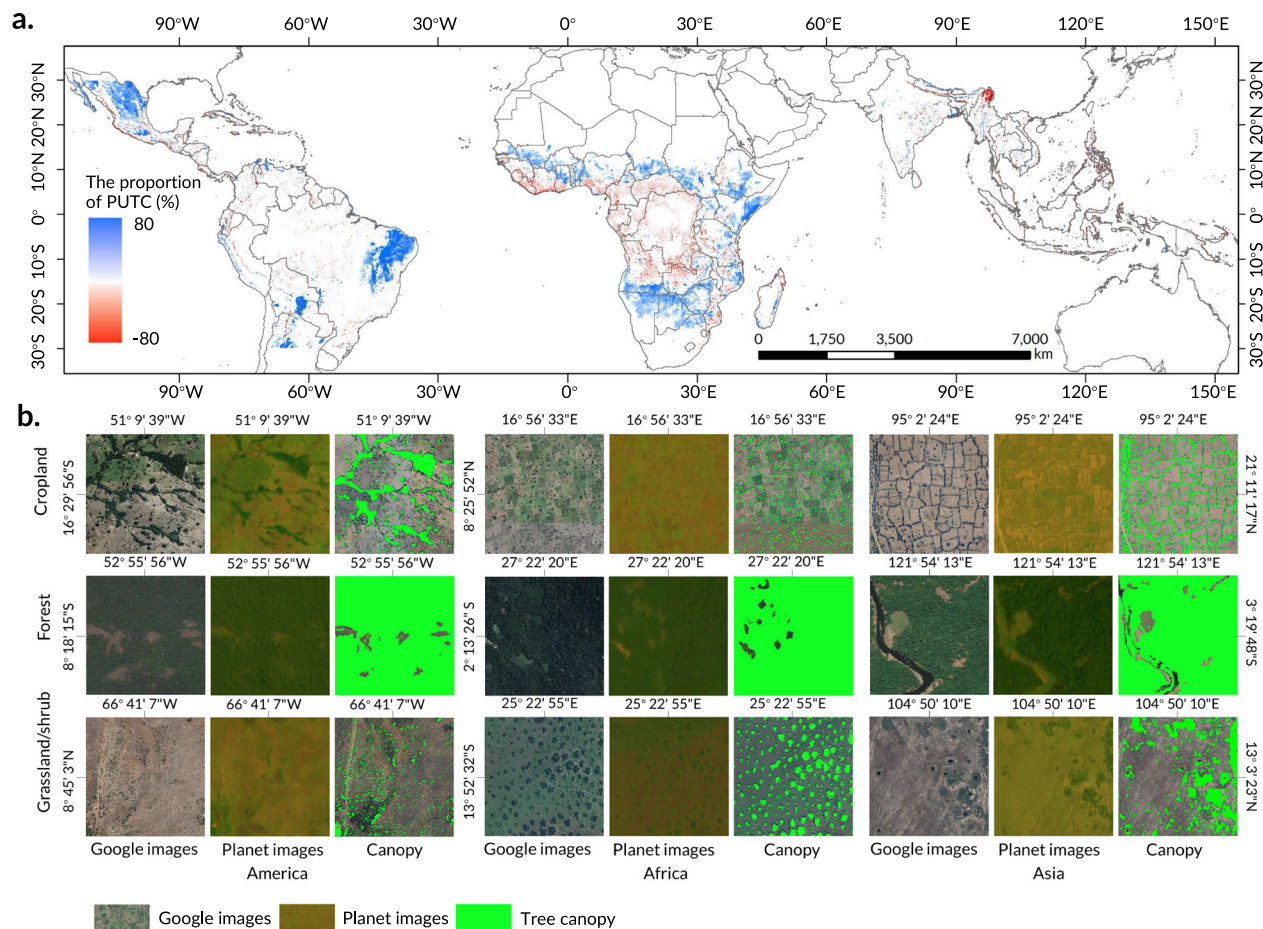


Fig. 2 | Distribution of high-resolution PUTC. **a** is the spatial distribution of the proportion of PUTC. **b** is the PUTC of a typical regional case. Data for this figure are available at Zenodo (<https://doi.org/10.5281/zenodo.14892757>).

edges ($PUTC < 0$; classified as forest grids, accounting for over 26.00% of total grid numbers. Figure 4d) and in non-forest grids with high PUTC ($PUTC > 0$; classified as non-forest grids, accounting for over 51.54% of total grid numbers. Figure 4b–f).

Given the spatial coherence between tree cover changes and PUTC, we quantified the driving factors behind tree cover changes (see Supplementary Fig. 3). Significant spatial disparities in tree cover are evident under different human activities and climatic conditions (see Supplementary Fig. 3a, b). Regarding spatial distribution, tree cover initially increases and then decreases with rising population density, peaking at a threshold population density of 23 per/km² (see Supplementary Fig. 3a). As precipitation increases, tree cover exhibits a trend of initial growth, stabilization, and subsequent growth across different grid types (see Supplementary Fig. 3b). Notably, the relationship between human activities, climate change, and tree cover varies (see Supplementary Fig. 3c). Precipitation and its fluctuations demonstrate a significant positive correlation with tree cover across all grid types. However, population density and its fluctuations only exhibit a significant positive correlation with tree cover in cropland grids and built-up area grids.

Furthermore, we analyzed the driving contributions of climate change, human activities, and LUCC to tree cover changes across different grid types (see Fig. 4g). Considering the high complexity of LUCC, including disturbances, we use the residual method to determine the contribution of LUCC (in Method section). From 2015 to 2022, LUCC played a dominant role in pan-tropical tree cover dynamics. Specifically, 53.93% of tree cover loss was related to LUCC, where lands have been continually modified throughout

deforestation. Meanwhile, climate change, represented by precipitation changes, is related to 43.98% of tree cover gain. Additionally, 2.10% of tree cover loss is linked to human activities. For different grid types, human activities were linked to 60.43% of tree cover loss in cropland grids and 53.22% of tree cover loss in built-up area grids. The increase in precipitation was related to tree cover gain across all grid types: cropland (28.58%), forest (36.64%), shrub/grassland (33.03%), bare land/desert (54.85%), and built-up area (8.54%). The LUCC played a dominant role in tree cover changes in built-up area grids and cropland grids, related to 38.25% and 10.99% of tree cover gain respectively, where the cropland and built-up areas expanded. Conversely, LUCC was related to tree cover loss in forest grids (61.33%), shrub/grassland grids (64.48%), and bare land/desert grids (44.51%). Anthropogenic impacts, including LUCC and human activities, exhibit an inverse relationship with pan-tropical tree cover changes compared to climate change. The increase in tree cover associated with heightened precipitation is offset by anthropogenic impacts.

Discussion

We have developed a high-resolution tree crown identification method based on machine learning to identify a large number of overlooked trees. In high-resolution satellite image identification of tree crowns, some studies have shown that machine learning, including deep learning, combined with very-high-spatial resolution satellite imagery collectively represents a disruptive technology that delivers excellent models for detecting isolated trees over large areas¹⁰. Undeniable, the transferability of the model across regions can be low, and had to use a

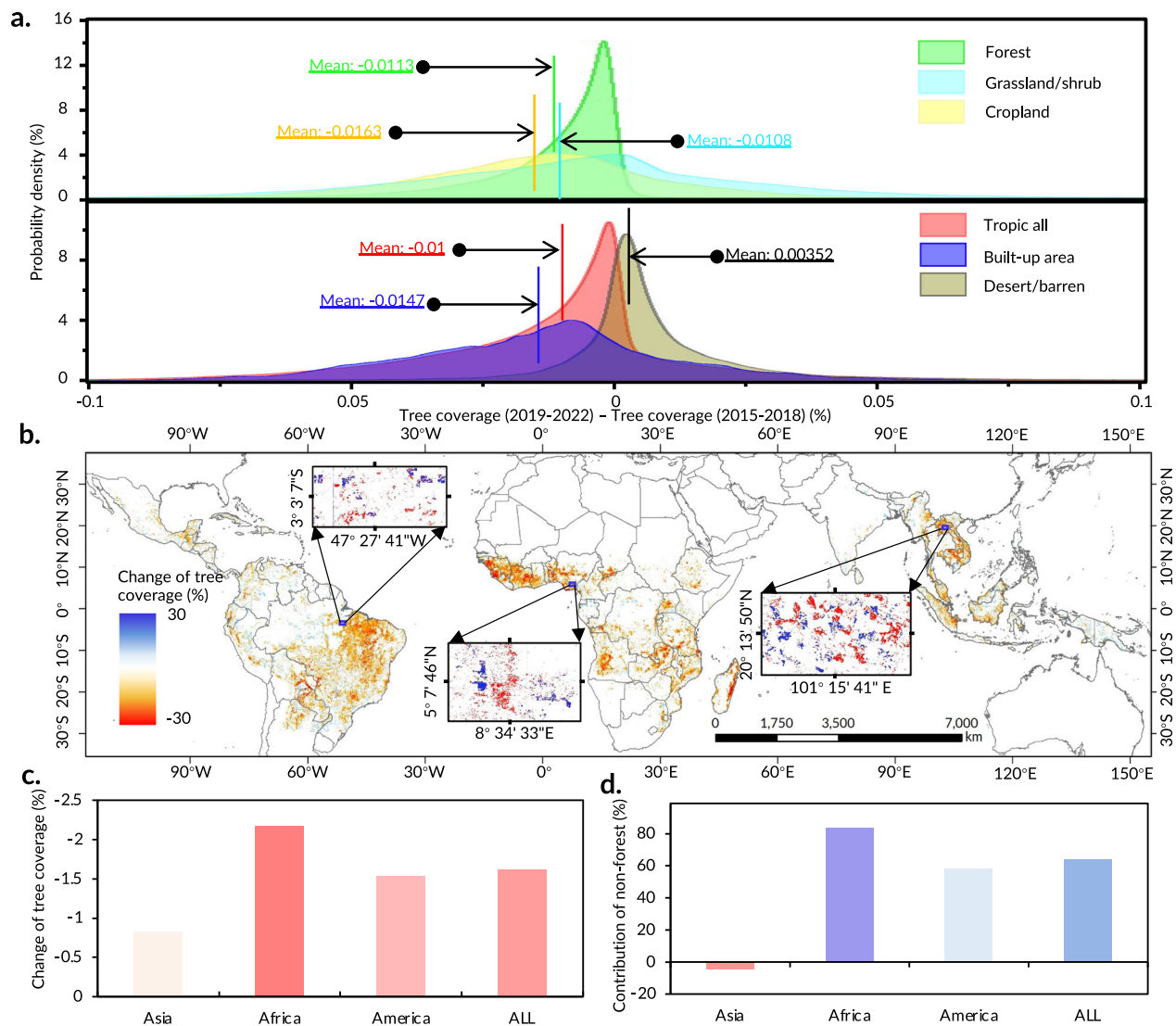


Fig. 3 | The spatiotemporal change of tree cover. **a** is the change of tree cover in different grid types from 2015 to 2022. **b** is the spatial distribution of tree cover changes. **c** is the change in tree cover in different regions from 2015 to 2022. **d** is the

contribution of non-forest grids to the change of tree cover. Data for this figure are available at Zenodo (<https://doi.org/10.5281/zenodo.14892757>).

very large number of training samples to achieve a high quality across landscapes¹⁰. Training samples also had to cover a range of different satellite images: acquisition dates, dust, clouds, burned areas, solar zenith and viewing angle, off-nadir, sensor systems and image boundaries all affect the visibility of tree crowns. All of these variations need to be taken into account when training the model, which requires a vast amount of training data and makes training time-consuming. Our combination of automatic sampling technology and machine learning provides a solution to this problem. The automatic sampling and cleaning of tree cover samples not only enhances the objectivity, but greatly saves human resources and time consumption. Due to our use of grid-by-grid stratified sampling, and the feature indicators used for cleaning samples are based on the prominent background features of the tree crown within each grid, our model has good transferability throughout the entire pan-tropical region (see Supplementary Note 1). Meanwhile, the combination of this solution with existing cloud computing platforms provides a path for achieving large-scale and fast high-resolution tree cover mapping. By comparison, it was found that our PUTC mapping results are highly consistent with Reiner's 1 m high-

resolution tree outer forest maps based on deep learning¹¹ (see Supplementary Fig. 4). Through error tracing analysis, although the error is small, nearly 90% of the error mainly occurs within the shrub/grassland grid (see Supplementary Fig. 6). It is undeniable that distinguishing tree crowns from a large number of sparse shrubs in Africa is difficult for remote sensing images with a resolution of 5 m, which is also the reason why our tree cover recognition results are higher in shrubs/grasslands ($r = 0.58$, $rmse = 9.49\%$, $bias = -3.96\%$) (see Supplementary Fig. 5). On a continental scale, the PUTC we detected is consistent with the current high-resolution trees outside forests recognized in Africa (see Supplementary Fig. 4). Notice that essentially, the limitation and challenge of this method in large-scale tree crown mapping is the need for global free and available high-resolution remote sensing images. This study was conducted with the support of Norway's International Climate and Forests Initiative Satellite Data Program, obtaining images with a resolution of < 5 meters covering the entire pan-tropical region. If free, high-quality global images can be obtained in the future, this method can provide technical support for the global rapid tree cover mapping.

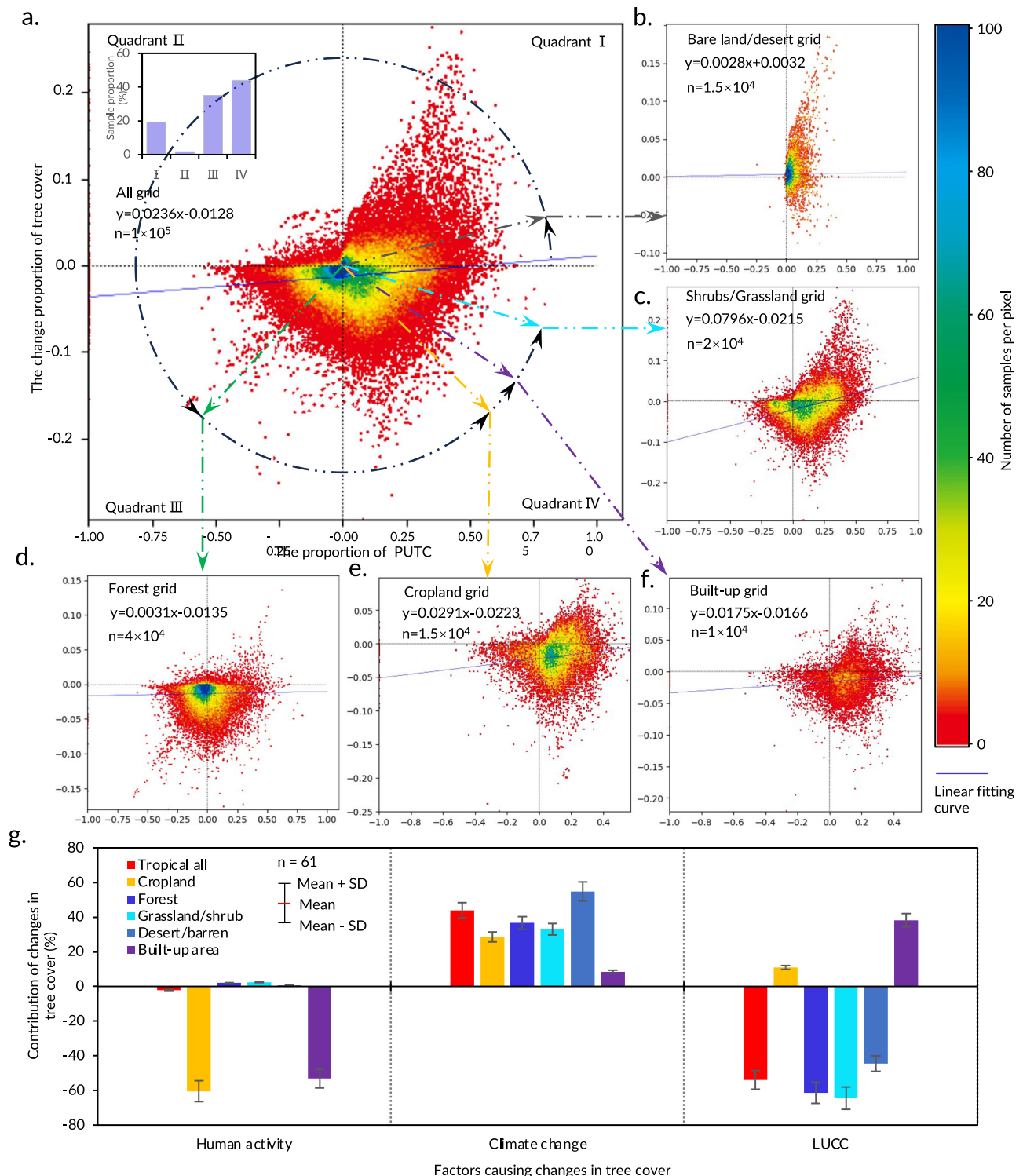


Fig. 4 | The contribution of driving factors for changes in tree cover. **a** is the relationship between the change of tree cover and the proportion of PUTC in pan-tropical, where the directions of the arrows represent the offset direction of the average coordinates of the samples in a specific grid type relative to the coordinate origin (0, 0), representing the main location of the samples of that type. **b–f** represents the relationship between the proportion of tree cover changes and

the proportion of PUTC within different types of grids. **g** shows the contributions of human activities, climate change, and LUCC to the changes in tree cover in the pan-tropical region. This result was calculated from 61 independent samples selected at different spatial locations in the tropics. Data are presented as mean values \pm SD. Data for this figure are available at Zenodo (<https://doi.org/10.5281/zenodo.14892757>).

We find that 17.31% of tree cover is found outside of land classified as ‘tree cover’. These trees play a crucial role in ecological stability, local economies, livelihoods, and food security^{35,36}. Consequently, underestimating tree cover hampers our understanding of global

water, carbon, and energy cycles^{37,38}. Mapping of tree cover down to the level of individual trees can resolve ambiguities in forest definitions, providing a basis for international comparison and coordination of forest resources. Major international conventions depend on

accurate forest data, but the diversity of national forest definitions complicates the implementation of these conventions³⁹. The primary challenge is consistently assessing all tree and forest resources across countries and over time. However, shifting the focus to individual trees could offer a more accurate and universally applicable framework for assessing forest resources. Furthermore, our results differ from previous studies by including the full range of trees located in farmlands, urban areas, and fragmented landscapes, which may constitute the missing carbon sink^{40,41}. This expanded perspective offers an opportunity to maximize the socioecological advantages derived from trees, transcending the boundaries of conventional forests. These benefits comprise enhanced agricultural sustainability, contributions to climate change mitigation, and biodiversity conservation^{42,43}. Additionally, as spatial resolution in tree cover and individual tree mapping improves, a precise assessment of all tree-based ecosystems is possible at the continental scale. Fine-scale changes in tree cover (gains and losses) within established forests, although not constituting land cover conversion, can still impact biogeochemical and biophysical feedback^{44,45}. These changes should be considered in climate-smart forest management strategies. Quantifying trees outside traditional forests also has implications for open ecosystems, enabling assessments of woody encroachment and identifying areas where biodiversity is threatened by increasing woody cover⁴⁶.

Variations in tree cover among different states based on land use, for forest, cropland, and built-up area grids, with America having the highest tree cover, followed by Asia and Africa. Climate, specifically rainfall and its seasonal distribution, is a key determinant of tree cover⁴⁷. In South America, tree cover in arid regions is higher in areas with high year-to-year variability in rainfall⁴⁸. Conversely, Africa typically shows lower tree cover in regions with low rainfall and/or high seasonality of rainfall⁴⁹. The diversity of vegetation types is also related to tree cover. Large-sized trees, predominantly found in warm and wet environments, are generally assumed to be older⁵⁰. However, tropical forests have progressively lost old-growth areas, evidence from 2015 shows that wood harvest is a major driver of the age distribution in tropical forests⁵¹. Regions with more fragmented and younger tree populations generally have lower overall tree cover. Additionally, sustainable agricultural practices in some parts of the Americas and Asia, such as retaining trees in croplands for shelterbelts or ecological balance, are emphasized¹⁴. In contrast, African drylands primarily use cropland trees for food, fodder, shade, and fuelwood, these trees are usually widely spaced, resulting in lower tree cover in croplands⁵².

In the 26th UN Climate Change Conference of the Parties (COP26) in Glasgow in 2021, 141 countries committed to halt and reverse forest loss and land degradation by 2030^{53–55}. Our results detected a tree cover gross loss of over 2.94% (67.24 Mha) in the pan-tropical region, which seriously hinders the implementation of the Glasgow Pledge. For example, some tropical rainforest countries such as Brazil, Indonesia, and the Democratic Republic of Congo suffered gross losses of 11.42 Mha, 2.15 Mha, and 3.34 Mha, respectively. However, the progress of another project promoting forest growth, Bonn Challenge Pledges, seems to have not been as smooth either. The Bonn Challenge is a global goal to bring 150 Mha of degraded and deforested landscapes into restoration by 2020 and 350 Mha by 2030⁵⁶. In fact, between 2015 and 2022, the tree cover only gross gained by 6.19 Mha. Among the pan-tropical forest powers that have made commitments, Brazil has the largest gross gain in tree cover at only 1.36 Mha which is much lower than Brazil's commitment of 4.28 Mha⁵⁶. In addition, in Africa and Southeast Asia, a lot of tree cover gain occurs in plantations and fallow areas of shifting cultivation. Therefore, it is urgent to strengthen the monitoring and management of global tree cover.

Interestingly, our results show that areas with the most drastic changes in tree cover are associated with PUTC. Compared to previous forest change detection methods that can only detect large-scale forest patch changes, our research reveals the important role of neglected

processes such as planting, logging, death, and regeneration of individual trees in the process of tree cover changes. Tree cutting and planting mainly occur in small areas, which cannot be detected in low-resolution remote sensing images^{10,57}. In fact, the changes in tree crowns within most cities and farmland are single or small-scale. Some regional studies using higher-resolution satellite images have discovered the death of individual trees in forests³², confirming the pattern we observed. This discovery likely proposes new requirements for future land and forest management. Meanwhile, the decrease in forest tree density caused by the logging and death of scattered individual trees does not change the forest area but can substantially impact regional ecology, carbon storage, and climate change.

Our results also show that there is a threshold effect between climate and human influence on tree crown distribution. For the population density threshold (PT: 23 people/km²), when the population density is below the threshold, the population density is related to the livability of natural conditions. Humans tend to choose superior habitats, so areas with higher population densities generally indicate better living conditions⁵⁸, which are more suitable for tree growth, resulting in larger tree cover. When the population density equals the threshold, human disturbance and tree growth reach a balance, meaning the loss and gain of tree cover balance each other. When population density surpasses a certain threshold, the balance is disrupted, and increased human activities are associated with greater tree disturbance and decreased tree cover.

For climate thresholds, including the first (CT1: 750 mm) and second thresholds (CT2: 1300 mm), precipitation in arid areas (below CT1) is the main ecosystem impact factor, and increased precipitation is the core driving force for promoting tree growth. When precipitation is between CT1 and CT2, the impact of precipitation on tree growth balances with the impact of human activities on tree planting/cutting. In such balanced areas, increased precipitation not only promotes tree growth but also improves human livability, leading to increased tree cutting and achieving a dynamic balance⁴⁶. When precipitation exceeds CT2, a large number of trees grow in the pan-tropical region, mainly forming large-scale forests.

Notably, the uncertainty of our results may arise from three aspects: tree definition, tree cover identification, and the reference map for tree cover during the PUTC mapping process. The current definition of a tree is influenced by the size and height of the tree crown and further by the resolution of satellite images. In our study, a tree with a crown diameter greater than 5 meters was defined as a tree, based on the maximum resolution of our satellite imagery. Some studies using sub-meter-level satellite imagery or aerial imagery within a small area define a tree crown size of 2 meters as the recognition threshold^{11,57}. The difference in this definition results in differences. Differences in these definitions result in variations in the area and percentage of tree crowns detected at different resolutions. The accuracy of tree cover change depends on the accuracy of the two periods of tree cover before and after, and also depends on the availability and quality of remote sensing images. Issues with clouds, shadows, and missing images also introduce uncertainty, particularly because leaf density and tree crown shape vary seasonally¹⁰. To address this, we used the average tree crown percentages from the adjacent four years to improve trend detection stability. Meanwhile, we also adopted the widely recognized uncertainty analysis method for land use change to evaluate the accuracy and uncertainty of tree cover change⁵⁹. In fact, the evaluation results are positive, with tree cover change overall having high accuracy (92.47%) and low uncertainty ($\pm 0.1031\%$). Future availability of satellite data at a sufficient temporal frequency to derive seamless mosaics would eliminate this source of bias from our method. Additionally, due to image resolution limitations, crowns less than 5 m apart cannot be distinguished, resulting in slightly higher tree cover estimates in sparse forests and shrubs. Compared to general 30 m resolution forest maps and 10 m

tree cover maps, our tree cover estimates represent significant progress⁶⁰. As high-resolution remote sensing images become more available, this issue will no longer exist. It should be noted that Northern Africa and half of South Africa are not mapped in our study due to the lack of coverage in the NICFI PlantScope imagery.

Ultimately, a significant source of uncertainty in PUTC mapping stems from the accuracy of the reference dataset. Taking the main reference World Cover dataset in this study as an example, the uncertainty of PUTC obtained by using the design-based area estimation is only ± 1.33 Mha ($\pm 0.06\%$ of the total tree cover) (see Supplementary Note 3). Additionally, we employed CGLS-LC100 and MODIS MCD12Q1 Global Land Cover Products at varying resolutions to assess the consistency of PUTC and quantify its accuracy and uncertainty ($\pm 1.78\%$ of all tree cover). Obviously, the uncertainty of PUTC obtained based on the consistency of different reference datasets is greater than that calculated based on the design-based area estimation. This difference demonstrates that the term ‘previously undetected’ can be challenging to define empirically. Ultimately, this study adopted higher uncertainty calculation results to enhance the scientific validity of the research. Indeed, PUTC may vary across different global tree cover datasets due to differences in resolution and the accuracy of the tree cover maps. The accuracy of the reference tree cover map directly influences the mapping results of PUTC. To enhance the reliability of the conclusions, we utilized the currently available World Cover dataset, which has a relatively high resolution, for PUTC mapping.

The main contribution of this work is mapping high-resolution PUTC and its changes, and quantifying the contrasting contributions of human and climate factors to pan-tropical tree cover changes in forests and non-forests. Our most advantageous finding is that the proportion of PUTC is 17.31% in the pan-tropical tree cover. Notably, statistics on PUTC show that the World Cover dataset in forest grids has an overestimation of 0.43% tree cover, indicating that existing forest or tree cover contains a large number of non-tree patches. Meanwhile, the World Cover dataset in non-forest grids has left out 17.74% of tree cover. Statistical results show that the main PUTC exists in non-forest grids. The grid type with the highest proportion of PUTC is shrub/grassland (15.11%), followed by cropland (2.15%), bare land/desert (0.40%), and built-up area (0.08%). Secondly, the average proportion of tree cover in the pan-tropical region decreased by 0.01% between 2015 and 2022, with forest grids and non-forest grids contributing 63.93% and 36.07%, respectively. Notably, areas experiencing evident short-term tree cover changes were primarily located in forest edges grids with negative PUTC values ($>26.00\%$) and in non-forest grids with high PUTC values ($>51.54\%$). Additionally, we found a threshold effect of population distribution and climate characteristics on tree cover distribution. LUCC plays a dominant role in the dynamics of pan-tropical tree cover, accounting for 53.93% of total tree cover loss. In contrast, climate change, represented by precipitation, is associated with 43.98% of total tree cover gain. While increased precipitation promotes tree cover gain, anthropogenic impacts counteract this trend, ultimately linking to net loss of tree cover.

Methods

Overview

This study establishes a framework for the detection of tree crowns using high spatial resolution remote sensing images. We employed an automated machine learning approach to identify pan-tropical tree crowns in Planet images with a 5 m spatial resolution. This approach differs from the typical Automated Machine Learning (AutoML) methods often referenced in computer science, as it focuses on achieving automatic sampling to reduce manual labor. Due to the unique vegetation features of pan-tropical trees, their crowns stand out as objects with a high NDVI and low brightness and wetness values, in contrast to their surroundings, which exhibit low NDVI and high brightness and wetness values. The significant differences in spectral

characteristics between tree crowns and non-tree crowns on the same plot will not rapidly weaken with differences in spatial location, remote sensing image capture time, and image quality (at least visually recognizable tree crowns) (see Supplementary Note 4). This study fully utilizes this feature to assist in identifying potential tree covers. We only need to focus on the differentiation between trees and non-trees within each plot (grid 500×500 m), without considering the consistency of tree crowns between different regions. This makes it possible for computers to automatically produce high-quality training samples based on each plot. Visually, it is straightforward to identify tree crowns in the satellite images, and we automatically delineated potential tree crowns. The strict cleaning and screening of a large number of automatically generated samples enable machine learning models to achieve high-quality learning.

For transferability, some studies acknowledge that the accuracy of deep learning heavily relies on samples^{11,14,29}. Due to the influence of the selected samples, deep learning models may experience errors in training the model due to regional or remote sensing image differences, thereby limiting its transferability²⁹ (see Supplementary Note 1). Although research cases in India have shown that this error can be reduced by increasing the sample size, it will significantly increase labor and computational costs¹⁴. Therefore, improving the large-scale applicability and transferability of the model is also an important prerequisite for achieving rapid global tree cover mapping. This study fully considers the significant differences in climate regions, ecosystem types, and human management, as well as the spatiotemporal heterogeneity of remote sensing images. A sufficient number of samples were automatically generated in different grids to improve the model's adaptability, transferability, and accuracy in mapping results across a large geographic range.

To achieve the above functions, this study considers model deployment on GEE and adopts the most widely used random forest algorithm as the core machine learning model. Considering the regional differences of the samples, we have developed an automatic sampling and sample cleaning method based on the potential crown to generate 500 almost accurate sample points within each 500×500 m grid. These samples were used to train the machine learning model, which was subsequently used to predict crowns for the entire pan-tropical region, capturing the full spatial variation and temporal change from 2015 to 2022. Finally, we investigated the contribution of factors such as precipitation, population, and land use to the spatiotemporal change of tropical tree cover.

Satellite images

We assembled all NICFI mosaics available on the GEE platform from 2015 to 2022. These images were obtained through the GEE license from the Norwegian Agency for Development Cooperation. All multi-spectral bands associated with the images were preprocessed on the GEE platform, including calibration and splicing. We formed the NDVI and NDWI from every image in the traditional way, from the pan-sharpened red and near-infrared bands, and formed the Brightness, Greenness, Wetness and Angle from every image in the improved Kirchhoff transform (KT). For Landsat satellite TM images, the KT band can effectively identify trees and forests, and its calculation requires B1–B6 and B7 (see Supplementary Note 4). Here, all KT bands are used from RGB, N (see Supplementary Eq.(7)). We also associated the multi-spectral bands with the NDVI band and KT bands, and ensured these basic feature bands were highly co-registered. These basic features were used to distinguish tree crowns from non-vegetated backgrounds.

A set of decision rules was applied to select images for the mosaic. The dry season is the season when tree crowns are most clearly distinguished. We used imagery collected all year, because of significant dry differences in the pan-tropical region. The first round of scoring considered the percentage of cloud cover, giving preference to

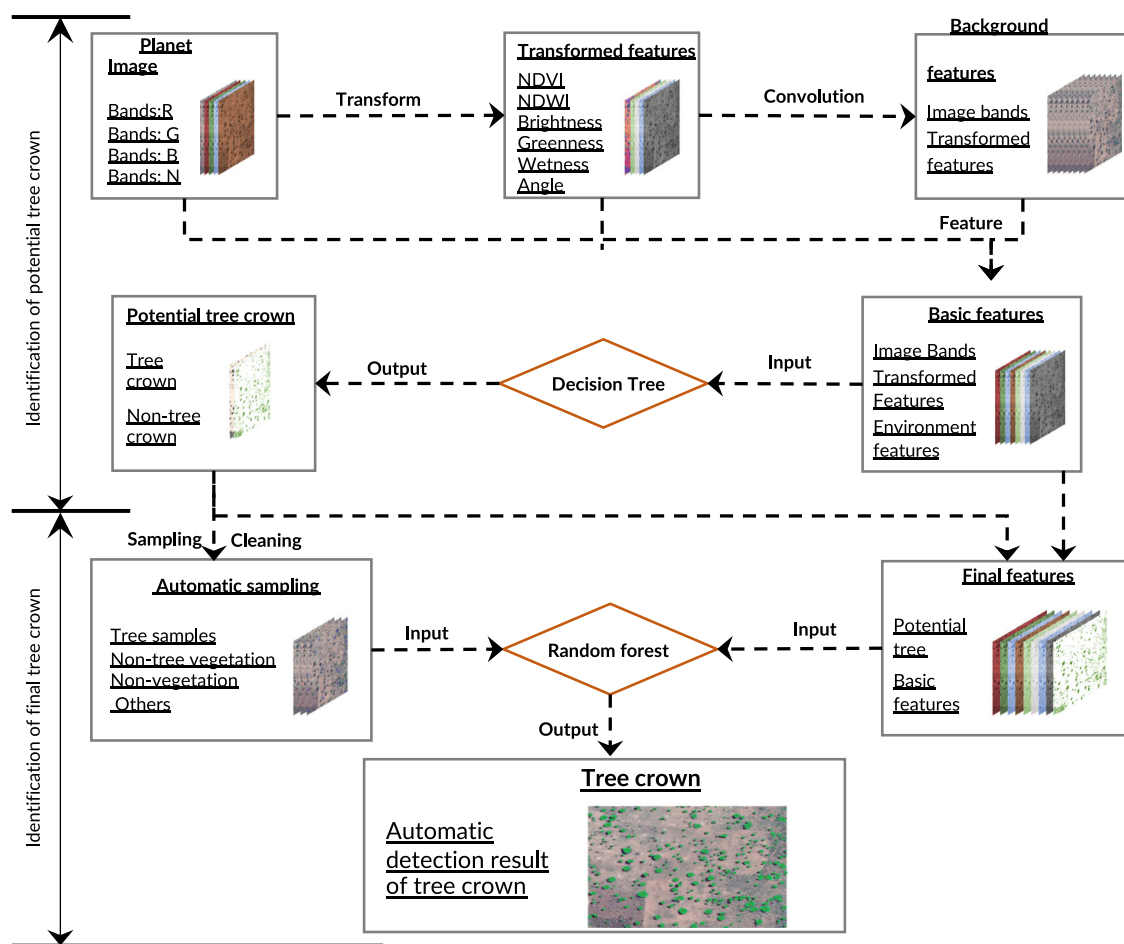


Fig. 5 | Automatic detection algorithm for tree crown. Data for this figure are available at Zenodo (<https://doi.org/10.5281/zenodo.14892757>).

imagery with lower cloud cover percentages. Image mosaics were necessary to eliminate the multiple counting of trees. For different time images of the same region within a year, to ensure the best selection of dry season images, we adopted a fusion method based on the minimum NDVI value. This resulted in images each year that were used for the study. Overall, 1% of the study area has been masked owing to insufficient data quality. Because most of these areas are located in the desert with very low tree cover, we do not expect any effect on the statistics presented.

Automatic detection algorithm

Our interactive tree cover automatic detection framework is based on the fusion of three technologies: decision tree classification, automatic clustering of random sample points, and machine learning (see Fig. 5).

Decision tree classification

We tentatively set a 20×20 convolutional kernel with weights of $1/400$, and calculate the background values for each KT band separately. This is equivalent to calculating the mean within a range of 100×100 m around each pixel. Due to the spatial distribution of trees in non-forest areas, the background, and mean values of each band, differ significantly from the characteristic parameters of the tree crown pixels. So, we reflect the prominent position of tree crowns in the surrounding background vegetation by using the difference between background values and corresponding KT band values, which includes two environmental indicators: KT Brightness (Envi-KTB) and KT Wetness (Envi-KTW). Obviously, the Envi-KTB and Envi-KTW in the tree crown area are negative and lower than the pixel values of the surrounding background. We associated the multispectral bands with

the NDVI band, KT bands, Envi-KTB and Envi-KTW, and formed these basic feature bands to distinguish tree crowns from non-vegetated background (see Supplementary Note 4).

We have set decision tree identification rules for single tree areas and dense tree areas respectively. It needs to be declared that the decision tree classification not align with the typical machine learning, as it involves a series of rules and conditions for categorization rather than traditional supervised learning for classification. In areas dominated by single/row trees, to ensure that almost all tree crowns are identified as potential tree crowns, we tentatively set two parallel judgment conditions. We determined the tree crown threshold under different conditions by analyzing the distribution characteristics of band information from 1,50,000 sample points (see Supplementary Note 5). Condition 1: Envi-KTB is less than 5% of the maximum Brightness value within each grid; Envi-KTW is less than 5% of the maximum Wetness value within each grid; NDVI value greater than 0.3; NDWI is less than -0.2 (excluding water). Condition 2: Envi-KTB is less than 10% of the maximum Brightness value within each grid; Envi-KTW is less than 10% of the maximum Wetness value within each grid; NDVI value greater than 0.15 (minimum identified NDVI of tree crowns in desert areas); NDWI is less than -0.2 . When either condition 1 or condition 2 is met, the algorithm automatically determines that the pixel belongs to the potential crown.

For the dense tree area, we first divide it into different coverage areas using the World Cover land cover dataset (10 m). Due to the inconsistent characteristics of tree crowns and background in different land types. Within the existing tree cover areas, all are assumed to be potential tree crowns. Within the cropland areas, the rule requires KT-Angle to be greater than the sum of KT-Greenness and KT-Brightness,

and NDVI to be greater than 0.75 (3/4 percentile of the total NDVI range). In built-up areas, NDVI is required to be greater than 0.7. In grasslands/shrubs, NDVI is required to be greater than 0.35. In bare land/deserts, NDVI is required to be greater than 0.25. Finally, by merging the distribution of different types of potential tree crowns, a potential tree crown dataset for the entire pan-tropical region is obtained.

Automatic clustering of random sample points

From the potential crown dataset, a stratified sampling method automatically extracts 500 sample points in each 500×500 m grid, consisting of 200 crown types and 300 non-crown types. Given the possible errors in tree crown identification, thorough cleaning of samples is necessary. This involves calculating the distribution of various eigenvalues for 300 tree samples and applying rigorous criteria to exclude uncertain samples: NDVI greater than Mean+0.5 standard deviation; Envi-KTB less than Mean+0.5 standard deviation; and Envi-KTW less than Mean+0.5 standard deviation (Supplementary Note 6). Only tree crown samples satisfying all these conditions are retained. For non-crown samples, the study excludes those with NDVI greater than Mean+3 standard deviations due to their heterogeneity. Cleaned non-crown samples are categorized into three types: non-vegetation (NDVI less than Mean+1 standard deviation) and non-tree vegetation (Mean+1 standard deviation \leq NDVI \leq Mean+3 standard deviations) (see Supplementary Note 6). Ultimately, three types of cleaned samples are identified: tree crown, non-tree vegetation, and non-vegetation. Through manual interpretation of 7500 real labels via Google Images, we've confirmed the automated labeling accuracy is consistently near 100%, with a sensitivity of zero (see Supplementary Note 7).

Mapping crown cover with machine learning

We used the most common supervised classification method in random forest algorithm, to detect tree crowns in the input images. The mapped areas were then converted to 0–1 images for counting the percentage of tree crowns in each 500×500 m grid. Machine learning has been the main driver of progress in artificial intelligence over the past decades. It emerged from research in artificial neural networks and refers to building models organized in layers of computational units, which develop more and more abstract representations of the underlying input data. After solving the problem of automatic precise sampling, we expect disruptive progress in remote sensing.

For data preparation, we assembled all NCFI mosaics available on the GEE platform into high-quality annual images from 2015 to 2022. For the labeling of the sample set, we adopt a computer automatic labeling method based on the combination of potential tree crown recognition results and sample cleaning methods. The method automatically generates 500 samples within each grid based on the proportion of potential tree cover, and labels them as tree crown and non-tree crown. In the sample cleaning stage, to improve the accuracy of the model and reduce the impact of non-tree vegetation on the tree crown, we reclassified high NDVI samples (greater than 3 Std) in non-tree samples as non-tree samples in vegetation. After strict sample cleaning, three types of labels are finally formed: tree crown samples, non-tree samples in vegetation, and non-tree samples in non-vegetation, which are then input into a random forest model for learning and classification. The automatically generated samples here are 100% used for model training. In determining the decision variables for the random forest model, we selected several spectral and environmental indices with the most distinct crown features and the greatest differences compared to non-trees, mainly including image bands (R, G, B, N), transformed features (NDVI, NDWI, brightness, wellness, angle), environmental features (envi-KTB, envi-KTW), and potential tree. Finally, we obtained high-resolution pan-tropical tree crown mapping results.

The model testing dataset consists of an additional 15,000 randomly selected validation points. We use visual interpretation to ensure the high accuracy of the test dataset by comparing it with Google Images. The validation process involves three remote sensing science interpreters who have worked continuously for over 500 h. To ensure consistency of the validation results throughout the entire study area, the same sample type was completed by the same interpreter. Three interpreters respectively validated samples with changes in tree crown, samples without changes in tree crown, and samples without tree crown. For the sample of a single tree, we used Google imagery that was as consistent as possible with the study date for validation. If there are no available Google images, we mark the sample as -1, indicating that the sample cannot be verified. For large-scale tree crowns, such as forests, we prioritize using Google imagery for validation. If no Google imagery is available, we will use contemporaneous Sentinel-2 imagery or Landsat imagery for validation. If both the Sentinel-2 image and the Landsat image are obscured by clouds or cannot be determined, the sample is marked as -1. Out of ~15,000 samples, 10% were marked as -1 and discarded.

Meanwhile, each grid is assigned land type attributes based on MCD12Q1 Global Land Cover Products³². We also collected and counted the percentage of tree covers that have been detected within each grid in the World Cover dataset (10 m). We then obtained the proportion of PUTC, by overlaying the existing tree cover. Noteworthy, some grids have negative PUTC values, especially in forest edge areas, indicating the presence of certain non-tree patches in forests detected by previous mid to low-resolution remote sensing images.

Overall, the model of this study has higher accuracy (see Supplementary Table 1). Meanwhile, the comprehensive sensitivity evaluation of the entire model shows that the mapping results have high stability (see Supplementary Note 7) under the current parameter settings. The detailed sensitivity and accuracy analysis of the first stage shows that the accuracy of potential crown recognition has a high stability (sensitivity of 0), which maintains the accuracy and stability of the overall model mapping results at over 95% (see Supplementary Note 7). For the sample cleaning stage and the tree crown mapping stage based on the random forest model, we evaluated the accuracy and sensitivity of the final tree crown mapping results for different samples under different cleaning intensities by adjusting the sample cleaning indicators (the degree to which the sample deviates from the mean, measured in standard deviation). The sensitivity analysis results in the final stage show that the mapping accuracy of the tree crown also has high stability (see Supplementary Note 7). These sensitivity assessment conclusions demonstrate the high reliability of our model for crown recognition.

Mapping crown cover change and PUTC

It is crucial to ensure the stability and comparability of tree cover datasets from different years when exploring the trend of tree cover changes in pan-tropical trees between 2015 and 2022. To improve comparability, we used the same algorithm to calculate the tree cover dataset for these years. To improve the accuracy of the change trend, we calculated the average tree cover percentage for each grid for 4 consecutive years, including early tree cover: 2015–2018 and later tree cover: 2019–2022. Determine the trend of change by calculating the difference between the early tree cover and the later tree cover. The entire process was completed jointly on the ArcGIS 10.2 and GEE. Meanwhile, we referred to the general accuracy, uncertainty, and bias analysis methods of forest change detection to calculate the accuracy and uncertainty of tree cover changes in this study⁶. The uncertainty analysis shows that the uncertainty areas of Tree loss and Tree gain are ± 2.05 Mha and ± 2.56 Mha, respectively, accounting for $\pm 0.0896\%$ and $\pm 0.1118\%$ of the total tree cover area, respectively. The uncertainty of net change in tree cover is ± 2.36 Mha, accounting for $\pm 0.1031\%$ of the total tree cover (see Supplementary Note 2).

Then, we plotted the pan-tropical tree cover, and then mapped the proportion PUTC. It is important to acknowledge that the term ‘previously undetected’ can be challenging to define empirically. Notably, PUTC may differ across various global tree cover datasets due to variations in resolution and accuracy. To verify the accuracy and uncertainty of the PUTC identified based on the World Cover dataset in this study, we used existing tree cover datasets of different resolutions as references, including World Cover (10 m resolution), CGLS-LC100 (100 m resolution), MODIS MCD12Q1 Global Land Cover Products (500 m resolution), conducted consistency checks on the recognition results of PUTC. Meanwhile, we used the standard deviation of the consistency of PUTC under different references as the uncertainty of the PUTC mapping results in this study. The comprehensive verification results reveal that the accuracy of PUTC is 87.34%, and the uncertainty of the PUTC mapping results is $\pm 1.78\%$ (see Supplementary Note 8).

Driving factors for changes in tree cover

Methodologically, land cover products were matched pixel by pixel between the periods 2015–2018 and 2019–2022. Pixels exhibiting changes in land cover were categorized as LUCC trajectories, while those without changes were identified as stable land trajectories. The tree cover change observed within stable land trajectories is interpreted as a compounded effect of climate change and human-induced vegetation alterations. The human activities refers to the planting or cutting of individual trees within a fixed land type, indicating shifts in vegetation composition or structure, such as the alteration of individual trees within stable farmland areas¹⁴. Consequently, anthropogenic impacts encompass both LUCC and human-induced tree cover changes (see Supplementary Note 9). Specifically, we identified precipitation as the most critical factor influencing vegetation among climate change variables¹⁰. As such, we used precipitation as a proxy for climate change. Additionally, population density reflects the impact of human activities on vegetation⁶¹; therefore, we employed population density as a proxy for human-induced tree cover change. Consequently, we examined the contributions of various factors to changes in pan-tropical tree cover from three perspectives: climate change, LUCC, and human activities. We developed a contribution quantification method based on sensitivity coefficients (Eq. (1)). This method has been shown to effectively differentiate the contributions of climate change and human activities to changes in land vegetation^{62,63}. Compared to changes in precipitation and population density, LUCC exhibits significant complexity and diversity, making it challenging to quantify its contribution to tree cover changes. Therefore, using the sensitivity coefficient method, we applied the residual method to determine the contribution of LUCC (C_{LUCC}), that is, the contribution after removing the quantified impacts of climate ($C_{Climate}$) and human factors (C_{Human}) from the total change (ΔTC). The calculation of sensitivity coefficients for each variable is performed using a multiple linear regression model in SPSS. Given the assumptions required for multiple linear regression, we statistically examined the distribution characteristics of ΔTC . The statistical results indicate that ΔTC follows a normal distribution (see Supplementary Fig. 8).

$$\Delta TC = C_{Climate} + C_{Human} + C_{LUCC} = S_{Climate} \Delta C + S_{Human} \Delta M + C_{LUCC} \quad (1)$$

$$S_{Climate} = \frac{\partial \Delta TC}{\partial \Delta C} \quad (2)$$

$$S_{Human} = \frac{\partial \Delta TC}{\partial \Delta M} \quad (3)$$

Here, $S_{Climate}$ and S_{Human} represent the sensitivity coefficients of the tree crown change to climate change and human disturbance factors, respectively. Using the changes in precipitation (ΔC) and population

density (ΔM) as independent variables, these sensitivity coefficients and residual contributions, which is the contribution of LUCC (C_{LUCC}), were calculated through regression analysis using SPSS software.

We estimate the influences of different factors on tree crown changes by multiplying the sensitivity coefficient with the corresponding factor change (Eq.(4) and (5)).

$$C_{Climate} = S_{Climate} \times \Delta C \quad (4)$$

$$C_{Human} = S_{Human} \times \Delta M \quad (5)$$

Based on the absolute influences of different factors on tree cover changes, we calculate their relative contribution percentages separately. It cannot be ignored that there is offsetting between the contributions of different factors. For example, when the increase in precipitation causes the tree gain (+100 Mha) to be equal to the tree loss (−100 Mha) caused by human logging, the tree cover in the region shows no change (0 Mha). However, in reality, the actual change in tree crown is as high as 200 Mha ($|+100| + |-100| = 200$), and the effects of precipitation (+50% = +100/200) and human activities (−50% = −100/200) on tree crown changes have been ignored. Therefore, it is necessary to calculate the percentage contribution of different factors to tree cover change, which is the proportion of the signed actual contribution of a single factor to the absolute sum of the contributions of all factors. In the actual calculation process, we separately considered the positive and negative attributes of different factors and constructed the formula for calculating the absolute contribution rate (Eq.(6)).

$$\begin{cases} R_{Climate} = \frac{C_{Climate}}{|C_{Climate}| + |C_{Human}| + |C_{LUCC}|} \times 100\% \\ R_{Human} = \frac{C_{Human}}{|C_{Climate}| + |C_{Human}| + |C_{LUCC}|} \times 100\% \\ R_{LUCC} = \frac{C_{LUCC}}{|C_{Climate}| + |C_{Human}| + |C_{LUCC}|} \times 100\% \end{cases} \quad (6)$$

Here, $R_{Climate}$, R_{Human} and R_{LUCC} represents the impacts of climate change, human interference, and LUCC on the tree crown changes of pan-tropical regions.

Statistics & reproducibility

This study establishes a model for the detection of tree crowns using high spatial resolution remote sensing images. This model was used to predict crowns for the entire pan-tropical region, capturing the full spatial variation and temporal change from 2015 to 2022. Finally, we investigated the contribution of factors such as precipitation, population, and land use to the spatiotemporal change of tropical tree cover. All samples used for statistical analysis were randomly selected within the tropical range. No data were excluded from the analyses.

Reporting summary

Further information on research design is available in the Nature Portfolio Reporting Summary linked to this article.

Data availability

The tree cover in the World Cover dataset (10 m) used in this study can be directly obtained by calling ID ESA/WorldCover/v100 in GEE. The MODIS MCD12Q1 Global Land Cover Products in 500 m (LC_Type1) can be directly obtained by calling ID MODIS/061/MCD12Q1 in GEE. The population density data set used in this study is obtained from the Center for International Earth Science Information Network (<https://sedac.ciesin.columbia.edu/data/set/gpw-v4-population-density-rev11>), and can be directly obtained by calling id CIESIN/GPWv411/GPW_Population_Density in GEE. In terms of climate change, the precipitation data set used in this study is obtained from the Climate hazards group

infrared precipitation with station data (<https://climatedataguide.ucar.edu/climate-data/chirps-climate-hazards-infrared-precipitation-station-data-version-2>). The high-resolution tree cover and tree cover change datasets can be viewed and obtained here (<https://nicegee20200601.users.earthengine.app/view/treecover-change-5m-app>). The tree cover change data generated in this study have been deposited in the Figshare database through the following link <https://doi.org/10.6084/m9.figshare.26345623>. Data for each figure are available at Zenodo (<https://doi.org/10.5281/zenodo.14892757>).

Code availability

All the code involved in this study can be obtained on the Zenodo platform through the following link <https://doi.org/10.5281/zenodo.14892757>⁶⁴.

References

- Pan, Y. D. et al. A large and persistent carbon sink in the world's forests. *Science* **333**, 988–993 (2011).
- Saatchi, S. S. et al. Benchmark map of forest carbon stocks in tropical regions across three continents. *Proc. Natl Acad. Sci. USA* **108**, 9899–9904 (2011).
- Mitchard, E. T. A. The tropical forest carbon cycle and climate change. *Nature* **559**, 527–534 (2018).
- Qin, Y. W. et al. Carbon loss from forest degradation exceeds that from deforestation in the Brazilian Amazon. *Nat. Clim. Change* **11**, 442–448 (2021).
- Hansen, M. C. et al. High-resolution global maps of 21st-century forest cover change. *Science* **342**, 850–853 (2013).
- McNicol, I. M., Ryan, C. M. & Mitchard, E. T. A. Carbon losses from deforestation and widespread degradation offset by extensive growth in African woodlands. *Nat. Commun.* **9**, 3045 (2018).
- Brandt, M. et al. Satellite passive microwaves reveal recent climate-induced carbon losses in African drylands. *Nat. Ecol. Evol.* **2**, 827–835 (2018).
- Jiang, M. K. et al. The fate of carbon in a mature forest under carbon dioxide enrichment. *Nature* **580**, 227–231 (2020).
- Luo, Y. Q. & Niu, S. L. The fertilization effect of CO₂ on a mature forest. *Nature* **580**, 191–192 (2020).
- Brandt, M. et al. An unexpectedly large count of trees in the West African Sahara and Sahel. *Nature* **587**, 78–82 (2020).
- Reiner, F. et al. More than one quarter of Africa's tree cover is found outside areas previously classified as forest. *Nat. Commun.* **14**, 2258 (2023).
- Koch, T. L., Perslev, M., Igel, C., Brandt, S. S. & Ieee. Accurate segmentation of dental panoramic radiographs with U-NETS. *16th IEEE International Symposium on Biomedical Imaging (ISBI)*. 15–19 (IEEE, 2019).
- Hanson, M. A. et al. Crystal structure of a lipid g protein-coupled receptor. *Science* **335**, 851–855 (2012).
- Brandt, M. et al. Severe decline in large farmland trees in India over the past decade. *Nat. Sustain.* **7**, 860–868 (2024).
- Brandt, M. et al. Woody plant cover estimation in drylands from Earth Observation based seasonal metrics. *Remote Sens. Environ.* **172**, 28–38 (2016).
- Ickowitz, A., Powell, B., Salim, M. A. & Sunderland, T. C. H. Dietary quality and tree cover in Africa. *Glob. Environ. Change Hum. Policy Dimens.* **24**, 287–294 (2014).
- Engert, J. E. et al. Ghost roads and the destruction of Asia-Pacific tropical forests. *Nature* **629**, 370–375 (2024).
- Ma, J., Li, J., Wu, W. & Liu, J. Global forest fragmentation change from 2000 to 2020. *Nat. Commun.* **14**, 3752 (2023).
- Bourgoin, C. et al. Human degradation of tropical moist forests is greater than previously estimated. *Nature* **631**, 570–576 (2024).
- Flores, B. M. et al. Critical transitions in the Amazon forest system. *Nature* **626**, 555–564 (2024).
- Gomes, V. H. F., Vieira, I. C. G., Salomão, R. P. & ter Steege, H. Amazonian tree species threatened by deforestation and climate change. *Nat. Clim. Change* **9**, 547–553 (2019).
- Cano, I. M. et al. Abrupt loss and uncertain recovery from fires of Amazon forests under low climate mitigation scenarios. *Proc. Natl Acad. Sci. USA* **119**, e2203200119 (2022).
- Staal, A. et al. Forest-rainfall cascades buffer against drought across the Amazon. *Nat. Clim. Change* **8**, 539–543 (2018).
- Curtis, P. G., Slay, C. M., Harris, N. L., Tyukavina, A. & Hansen, M. C. Classifying drivers of global forest loss. *Science* **361**, 1108–1111 (2018).
- Feng, Y. et al. Doubling of annual forest carbon loss over the tropics during the early twenty-first century. *Nat. Sustain.* **5**, 444–451 (2022).
- Choat, B. et al. Global convergence in the vulnerability of forests to drought. *Nature* **491**, 752–755 (2012).
- Funk, C. et al. The climate hazards infrared precipitation with stations—a new environmental record for monitoring extremes. *Sci. Data* **2**, 150066 (2015).
- Yang, F. & Zeng, Z. Z. Refined fine-scale mapping of tree cover using time series of Planet-NICFI and Sentinel-1 imagery for Southeast Asia (2016–2021). *Earth Syst. Sci. Data* **15**, 4011–4021 (2023).
- Tolan, J. et al. Very high resolution canopy height maps from RGB imagery using self-supervised vision transformer and convolutional decoder trained on aerial lidar. *Remote Sens. Environ.* **300**, 113888 (2024).
- Griscom, B. W. et al. Natural climate solutions. *Proc. Natl Acad. Sci. USA* **114**, 11645–11650 (2017).
- Goswami, S. et al. Decision trees within a molecular memristor. *Nature* **597**, 51–56 (2021).
- Friedl, M. A. et al. MODIS Collection 5 global land cover: algorithm refinements and characterization of new datasets. *Remote Sens. Environ.* **114**, 168–182 (2010).
- Zanaga, D. et al. ESA WorldCover 10 m 2020 v100. *European Space Agency*. <https://doi.org/10.5281/zenodo.5571936> (2021).
- FAO. Global Forest Resources Assessment 2020. <https://doi.org/10.4060/ca9825en> (2020).
- Hart, D. E. T. et al. Priority science can accelerate agroforestry as a natural climate solution. *Nat. Clim. Change* **13**, 1179–1190 (2023).
- Bayala, J., Sanou, J., Teklehaimanot, Z., Kalinganire, A. & Ouédraogo, S. J. Parklands for buffering climate risk and sustaining agricultural production in the Sahel of West Africa. *Curr. Opin. Environ. Sustain.* **6**, 28–34 (2014).
- yu, G. R., Chen, Z. & Wang, Y. P. Carbon, water and energy fluxes of terrestrial ecosystems in China. *Agr. Forest Meteorol.* **346**, 109890 (2024).
- Forzieri, G. et al. Increased control of vegetation on global terrestrial energy fluxes. *Nat. Clim. Change* **10**, 356–362 (2020).
- Zalles, V., Harris, N., Stolle, F. & Hansen, M. C. Forest definitions require a re-think. *Commun. Earth Environ.* **5**, 620 (2024).
- Leng, S., Sun, R. H., Yang, X. J., Jin, M. X. & Chen, L. D. Diverse types of coupling trends in urban tree and nontree vegetation associated with urbanization levels. *Npj Urban Sustain.* **3**, 33 (2023).
- Mugabowindekwe, M. et al. Trees on smallholder farms and forest restoration are critical for Rwanda to achieve net zero emissions. *Commun. Earth Environ.* **5**, 113 (2024).
- Ratnam, J. et al. Trees as nature-based solutions: a global south perspective. *One Earth*. **3**, 140–144 (2020).
- Sietz, D., Klimek, S. & Dauber, J. Tailored pathways toward revived farmland biodiversity can inspire agroecological action and policy to transform agriculture. *Commun. Earth Environ.* **3**, 211 (2022).
- Heinrich, V. H. A. et al. Large carbon sink potential of secondary forests in the Brazilian Amazon to mitigate climate change. *Nat. Commun.* **12**, 1785 (2021).
- Su, Y. X. et al. Asymmetric influence of forest cover gain and loss on land surface temperature. *Nat. Clim. Change* **13**, 823–831 (2023).

46. Venter, Z. S., Cramer, M. D. & Hawkins, H. J. Drivers of woody plant encroachment over Africa. *Nat. Commun.* **9**, 2272 (2018).
 47. Hirota, M., Holmgren, M., Van Nes, E. H. & Scheffer, M. Global resilience of tropical forest and savanna to critical transitions. *Science* **334**, 232–235 (2011).
 48. Holmgren, M., Hirota, M., van Nes, E. H. & Scheffer, M. Effects of interannual climate variability on tropical tree cover. *Nat. Clim. Change* **3**, 755–758 (2013).
 49. Staver, A. C., Archibald, S. & Levin, S. Tree cover in sub-Saharan Africa: rainfall and fire constrain forest and savanna as alternative stable states. *Ecology* **92**, 1063–1072 (2011).
 50. Au, T. F. et al. Younger trees in the upper canopy are more sensitive but also more resilient to drought. *Nat. Clim. Change* **12**, 1168–1174 (2022).
 51. McDowell, N. G. et al. Pervasive shifts in forest dynamics in a changing world. *Science* **368**, 964 (2020).
 52. Liu, S., Wang, L., Zhang, J. & Ding, S. Opposite effect on soil organic carbon between grain and non-grain crops: evidence from Main Grain Land. *China Agric. Ecosyst. Environ.* **379**, 109364 (2025).
 53. Gasser, T., Ciais, P. & Lewis, S. L. How the Glasgow Declaration on Forests can help keep alive the 1.5 °C target. *Proc. Natl Acad. Sci. USA* **119**, e2200519119 (2022).
 54. UKCOP26. Glasgow leaders' declaration on forests and land use. <https://ukcop26.org/glasgow-leaders-declaration-on-forests-and-land-use/> (2021).
 55. GOV.UK. Over 100 leaders make landmark pledge to end deforestation at COP26. <https://www.gov.uk/government/news/over-100-leaders-make-landmark-pledge-to-end-deforestation-at-cop26> (2021).
 56. IUCN. The bonn challenge. <https://www.bonnchallenge.org/> (2011).
 57. Cheng, Y. et al. Scattered tree death contributes to substantial forest loss in California. *Nat. Commun.* **15**, 641 (2024).
 58. Sullivan, A. P., Bird, D. W. & Perry, G. H. Human behaviour as a long-term ecological driver of non-human evolution. *Nat. Ecol. Evol.* **1**, 0065 (2017).
 59. Olofsson, P. et al. Good practices for estimating area and assessing accuracy of land change. *Remote Sens. Environ.* **148**, 42–57 (2014).
 60. Li, W. et al. Human fingerprint on structural density of forests globally. *Nat. Sustain.* **6**, 368–379 (2023).
 61. Tritsch, I. & Le Tourneau, F.-M. Population densities and deforestation in the Brazilian Amazon: New insights on the current human settlement patterns. *Appl. Geog.* **76**, 163–172 (2016).
 62. Zhang, J. & Liu, Y. J. Decoupling of impact factors reveals the response of cash crops phenology to climate change and adaptive management practice. *Agr. For. Meteorol.* **322**, 109010 (2022).
 63. Zhang, S. et al. Human interventions have enhanced the net ecosystem productivity of farmland in China. *Nat. Commun.* **15**, 10523 (2024).
 64. Liu, S. D. et al. Data and methodological support for mapping previously undetected trees reveals overlooked changes in pan-tropical tree cover. *Zenodo*. <https://doi.org/10.5281/zenodo.14892757> (2025).
- Science Foundation of China (Grant No: 42401082), Postdoctoral Fellowship Program of CPSF (Grant No: GZC20232757; GZC20240855), Project funded by China Postdoctoral Science Foundation (Grant No: 2024M763351), and Independent deployment project of the Chinese Academy of Sciences (Grant No: E4Z202021F). Additionally, we also want to thank the anonymous reviewers for their valuable suggestions and comments that contributed to improving the quality of the manuscript.

Author contributions

S.L., J.Z., L.W. and J.J.Z. conceived concepts and designed the study. S.L., J.Z. and L.W. performed the study. P.C., J.J.Z. and J.P. optimized the framework of this study. S.L., J.Z., P.C. and J.P. analyzed the contribution of different factors. B.N., I.J., X.W. and S.D. contributed to the validation of treecover mapping results. W.L., N.H., W.S., W.N. and Z.N. processed the land use/cover data and performed the subsequent analyses. S.L. and J.Z. wrote the manuscript. All authors discussed the results and commented on the manuscript.

Competing interests

The authors declare no competing interests

Additional information

Supplementary information The online version contains supplementary material available at <https://doi.org/10.1038/s41467-025-60662-z>.

Correspondence and requests for materials should be addressed to Li Wang or Jianjun Zhang.

Peer review information *Nature Communications* thanks the anonymous reviewers for their contribution to the peer review of this work. A peer review file is available.

Reprints and permissions information is available at <http://www.nature.com/reprints>

Publisher's note Springer Nature remains neutral with regard to jurisdictional claims in published maps and institutional affiliations.

Open Access This article is licensed under a Creative Commons Attribution-NonCommercial-NoDerivatives 4.0 International License, which permits any non-commercial use, sharing, distribution and reproduction in any medium or format, as long as you give appropriate credit to the original author(s) and the source, provide a link to the Creative Commons licence, and indicate if you modified the licensed material. You do not have permission under this licence to share adapted material derived from this article or parts of it. The images or other third party material in this article are included in the article's Creative Commons licence, unless indicated otherwise in a credit line to the material. If material is not included in the article's Creative Commons licence and your intended use is not permitted by statutory regulation or exceeds the permitted use, you will need to obtain permission directly from the copyright holder. To view a copy of this licence, visit <http://creativecommons.org/licenses/by-nc-nd/4.0/>.

© The Author(s) 2025

Acknowledgments

This work was supported by the National Key Research and Development Program of China (Grant No:2021YFE0117900), National Natural